

# Allostery and Kinetic Proofreading

## Supporting Information

Vahe Galstyan<sup>†</sup> and Rob Phillips<sup>\*,‡,¶,§</sup>

<sup>†</sup>Biochemistry and Molecular Biophysics Option, <sup>‡</sup>Department of Physics, <sup>¶</sup>Department of Applied Physics, and <sup>§</sup>Division of Biology and Biological Engineering, California Institute of Technology, Pasadena, California 91125, United States

\*E-mail: phillips@pboc.caltech.edu

## Contents

<b>A</b>	<b>Discrimination Fidelity in the Conceptual Scheme of the Piston Model</b>	<b>S2</b>
<b>B</b>	<b>Ratchet and Pawl Engine</b>	<b>S4</b>
B.1	Details of the Ratchet and Pawl Mechanism in the Absence of Piston Coupling	S4
B.2	Derivation of $\Delta W_{1/2}$ Expressions . . . . .	S6
<b>C</b>	<b>Equilibrium Properties of the Allosteric Enzyme</b>	<b>S8</b>
C.1	Constraints on the Choice of Enzyme's Rate Constants . . . . .	S8
C.2	Enzyme Fidelity at a Fixed Ligand Concentration . . . . .	S10
<b>D</b>	<b>Full Description of the Piston Model with Engine-Enzyme Coupling</b>	<b>S13</b>
D.1	Equilibrium Fidelity of the Piston Model in the Absence of External Driving	S13
D.2	Obtaining the Steady-State Occupancy Probabilities . . . . .	S16
D.3	Enzyme's Kinetic Parameters Used for the Numerical Study in Section 3.4 . .	S18
D.4	Details of the Numerical Optimization Procedure for Finding the Highest Fidelity . . . . .	S19
D.5	Investigation of the $\alpha_{\max} \approx 3$ Result for the Highest Available Proofreading	
	Index . . . . .	S20
	<b>References</b>	<b>S24</b>

# A Discrimination Fidelity in the Conceptual Scheme of the Piston Model

In this section, we derive the expressions for the fidelities achieved at the two piston steps introduced in section 2 of the main text, namely,  $\eta_1 = k_{\text{off}}^{\text{W}}/k_{\text{off}}^{\text{R}}$  when the piston is expanded, and  $\eta_2 = (k_{\text{off}}^{\text{W}} + r)/(k_{\text{off}}^{\text{R}} + r)$  when the piston is compressed. In our discussion, we retain the simplifying assumptions made during the presentation of the model concept.

As discussed in section 2, the first level of substrate discrimination occurs in the expanded piston state. If the waiting time for compression is long enough for the substrates to equilibrate with the inactive enzyme, we can impose the detailed balance condition at the two pairs of edges in Figure S1A to obtain

$$p_{\text{I}}^{\text{R}} k_{\text{off}}^{\text{R}} = p_{\text{I}} k_{\text{on}}[\text{R}], \quad (\text{S1})$$

$$p_{\text{I}}^{\text{W}} k_{\text{off}}^{\text{W}} = p_{\text{I}} k_{\text{on}}[\text{W}]. \quad (\text{S2})$$

Here  $p_{\text{I}}$ ,  $p_{\text{I}}^{\text{R}}$  and  $p_{\text{I}}^{\text{W}}$  stand for the probabilities of the empty, right substrate-bound and wrong substrate-bound inactive states of the enzyme, respectively. Taking the substrate concentrations to be identical ( $[\text{R}] = [\text{W}]$ ), we can equate the left sides of eqs S1 and S2 to find

$$\frac{p_{\text{I}}^{\text{R}}}{p_{\text{I}}^{\text{W}}} = \frac{k_{\text{off}}^{\text{W}}}{k_{\text{off}}^{\text{R}}}. \quad (\text{S3})$$

The above ratio of probabilities represents the proportion in which right and wrong substrate-bound inactive enzymes enter the active state, and therefore, becomes equivalent to the fidelity  $\eta_1$  achieved in the first discrimination step.

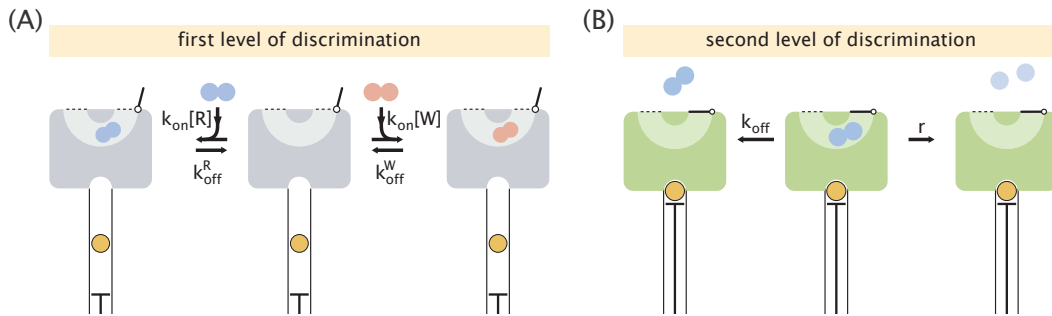


**Figure S1.** The two substrate discrimination levels in the conceptual scheme of the piston model. (A) The first level is achieved when the piston is expanded and a roughly equilibrium distribution of substrate-bound and free enzyme states is established. (B) The second level is achieved in the compressed state of the piston where the enzyme is active and can either release the bound substrate or turn it into a product.

The second level of substrate differentiation takes place when the piston gets compressed, leading to the activation of the enzyme. We assume that in its active state the enzyme can no longer bind new substrates. If we wait long enough, a substrate that was already bound before piston compression will either unbind with a rate  $k_{\text{off}}$  or get turned into a product

with a rate  $r$ . The probability that a product is formed can be written as

$$p_{\text{prod}} = \int_0^\infty dt' p_{\text{bound}}(t') \times r, \quad (\text{S4})$$

where  $p_{\text{bound}}(t')$  is the probability that the substrate is still bound by time  $t'$ . Using the fact that the waiting time distribution of substrate release (either through unbinding or product formation) is  $P_{\text{release}}(t) = (k_{\text{off}} + r)e^{-(k_{\text{off}}+r)t}$ , the probability  $p_{\text{bound}}(t)$  can be found as

$$p_{\text{bound}}(t) = \int_t^\infty dt' P_{\text{release}}(t') = e^{-(k_{\text{off}}+r)t}. \quad (\text{S5})$$

Substituting this result into eq S4 and performing the integration, we obtain

$$p_{\text{prod}} = \frac{r}{k_{\text{off}} + r}. \quad (\text{S6})$$

Due to the difference in the off-rates of the right and wrong substrates, their respective probabilities of production will also be different, resulting in the second level of fidelity given by the ratio of these probabilities, namely,

$$\eta_2 = \frac{p_{\text{prod}}^{\text{R}}}{p_{\text{prod}}^{\text{W}}} = \frac{k_{\text{off}}^{\text{W}} + r}{k_{\text{off}}^{\text{R}} + r}. \quad (\text{S7})$$

## B Ratchet and Pawl Engine

In this section, we first provide a detailed discussion of the ratchet and pawl mechanism in the absence of piston coupling. Then, for the case of piston coupling, we derive of the expressions for the work per step ( $\Delta W_{1/2}$ ) shown in Figure 3 at which the ratio of piston state probabilities ( $\pi_d/\pi_u$ ) and the net rate of backward stepping ( $k_{\text{net}}$ ) reach 50% of their respective saturation values.

### B.1 Details of the Ratchet and Pawl Mechanism in the Absence of Piston Coupling

The ratchet and pawl mechanism was originally proposed by Richard Feynman with an aim to demonstrate the validity of the second law of thermodynamics.<sup>1</sup> In his description, the mechanism had an additional element, namely, vanes that were connected to the ratchet through a massless axle (Figure S2A). The purpose of the vanes was to induce forward ratchet steps through thermal fluctuations. When the temperature in the vane compartment was maintained at a higher value than that in the ratchet compartment ( $T_2 > T_1$ ), the mechanism could utilize this difference to operate as a heat engine and lift a weight hanging from the axle.

In the piston model, instead of running the ratchet and pawl mechanism as a heat engine, we drive it at a constant temperature through the expenditure of the gravitational potential energy of the hanging weight. We have therefore removed the vane compartment from our description of the engine and ascribed forward stepping to random rotational fluctuations of the ratchet instead (Figure S2B).

As mentioned in section 3.1, backward stepping takes place whenever the pawl borrows sufficient energy from the environment to overcome the potential energy barrier  $E_0$  of the spring and lift itself over the ratchet tooth that it is sitting on, allowing the tooth to slip under it (Figure S2C). Once the pawl gets over the ratchet tooth (step 2 in Figure S2C), the hanging weight and the recovering pawl start applying torque on the ratchet, causing it to rotate in the clockwise direction (step 3 in Figure S2C). Following Feynman's treatment, we assume that when the pawl hits the bottom of the next tooth (step 4 in Figure S2C), the total kinetic energy of the system, which is the sum of the energy borrowed by the pawl and the change in the potential energy of the weight per step ( $\Delta W = mg\Delta z$ ), gets dissipated due to the perfectly inelastic collision of the pawl with the ratchet. Therefore, as a result of a single backward step, the net heat dissipated into the environment becomes  $\Delta W$ , as reflected in the free energy landscape in Figure S2E.

A similar set of arguments for forward stepping would imply that initially the mechanism needs to borrow enough energy from the environment to overcome the spring barrier and to lift the weight by an amount of  $\Delta z$  (step 3 in Figure S2D). We again assume, that once the pawl passes over the next tooth and inelastically hits the ratchet, it dissipates all its accumulated potential energy. Therefore, in the end of a single forward step, the total energy extracted from the environment is equal to the increase in the potential energy of the weight per forward step (Figure S2E).

Implicit in our treatment of ratchet stepping has been the assumption that we could discretize the possible configurations of the mechanism into states where the pawl fully rests

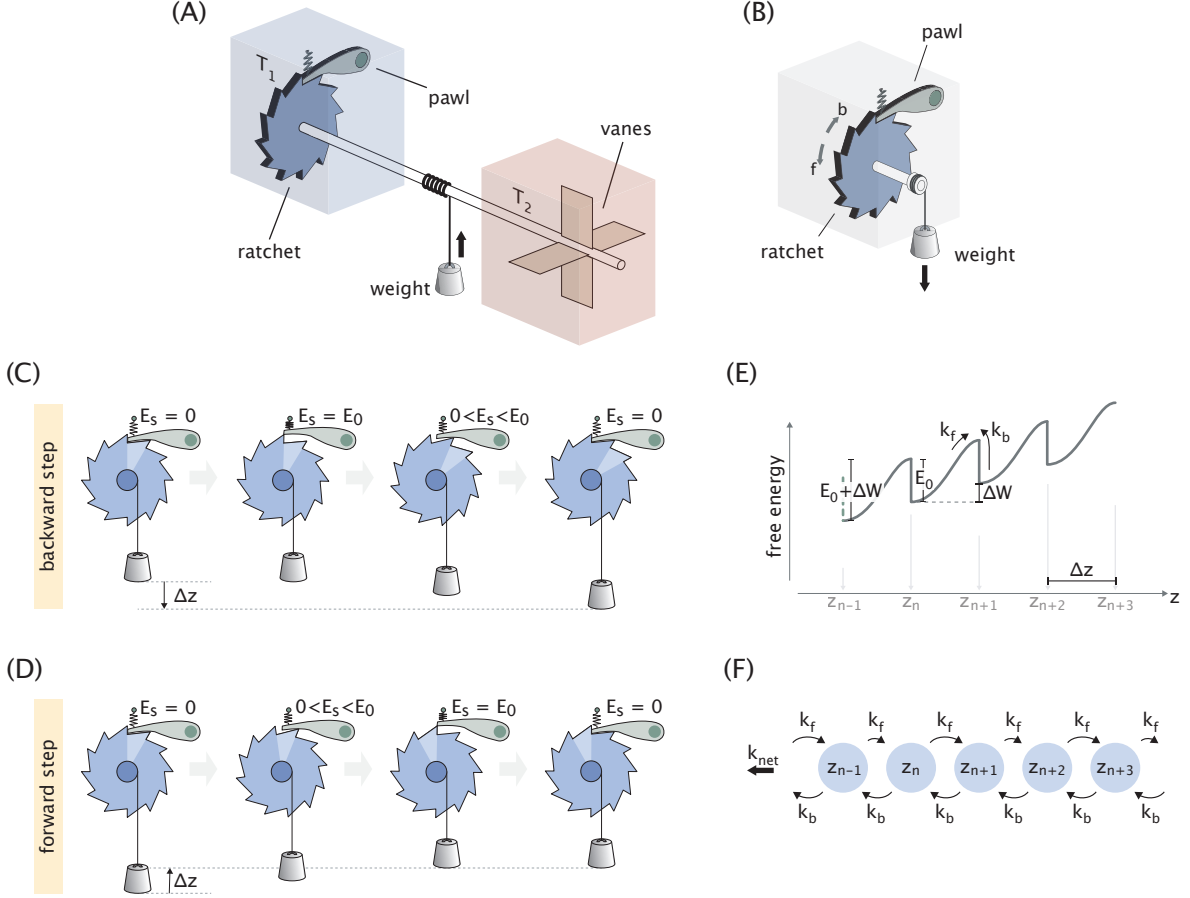


**Figure S2.** Working details of the ratchet and pawl mechanism. (A) Feynman’s original ratchet and pawl mechanism operating as a heat engine.<sup>1</sup> (B) Ratchet and pawl engine driven by a hanging weight that is used in the piston model. Arrows with symbols “b” and “f” indicate the directions of backward and forward ratchet rotation, respectively. (C)-(D) Breakdown of backward (C) and forward (D) steps of the ratchet, accompanied by the lowering or the lifting of the weight, respectively.  $E_s$  stands for the potential energy of the spring. (E) Free energy landscape corresponding to the directionally biased rotations of the ratchet due to a net lowering of the weight. Discrete positions of the weight ( $z_n$ ) corresponding to the energy minima of the landscape are marked on the reaction coordinate. (F) Infinite chain representation of the discrete state dynamics. When a non-zero weight is hung from the axle, the ratchet makes backward steps with a net rate  $k_{net}$ .

on ratchet teeth. Within this formalism, we took  $E_0$  to be the activation energy of backward stepping and  $(E_0 + \Delta W)$  to be the activation energy of forward stepping, resulting in rate constants given by

$$k_b = \tau^{-1} e^{-\beta E_0}, \quad (\text{S8})$$

$$k_f = \tau^{-1} e^{-\beta(E_0 + \Delta W)}, \quad (\text{S9})$$

where  $\tau^{-1}$  is the attempt frequency. The choice of identical attempt frequencies for forward and backward steps is, in a way, a requirement in the discretization formalism to ensure

that in the absence of driving ( $\Delta W = 0$ ) no net rotation of the ratchet is generated, since  $k_{\text{net}} = k_{\text{b}} - k_{\text{f}}$  (Figure S2F). We note that a more rigorous treatment of ratchet stepping kinetics would need to account for the precise shape of the energy landscape, defined both by the position of the weight (equivalently, the ratchet angle) and the angular position of the fluctuating pawl, similar to the analysis done by Magnasco and Stolovitzky.<sup>2</sup>

## B.2 Derivation of $\Delta W_{1/2}$ Expressions

We begin by deriving the  $\Delta W_{1/2}$  expression at which the ratio  $\pi_{\text{d}}/\pi_{\text{u}}$  is 1/2. From eqs 12 and 13, this ratio, evaluated at  $\Delta W_{1/2}$ , can be written as

$$\left. \frac{\pi_{\text{d}}}{\pi_{\text{u}}} \right|_{\Delta W_{1/2}} = \frac{1 + e^{-\beta(\Delta W_{1/2} + \Delta F)}}{1 + e^{-\beta(\Delta W_{1/2} - \Delta F)}} = \frac{1}{2}. \quad (\text{S10})$$

Solving for  $\Delta W_{1/2}$ , we obtain

$$\begin{aligned} \Delta W_{1/2} &= \Delta F + \ln(1 + e^{-2\beta\Delta F}) \\ &= \Delta F + \ln(1 + f^{-2}), \end{aligned} \quad (\text{S11})$$

where in the last step we used the expression for the ligand free energy change written in terms of the compression factor, that is,  $\Delta F = \beta^{-1} \ln f$ . Since for efficient proofreading the compression factor needs to be large ( $f \gg 1$ ), the  $\Delta W_{1/2}$  expression reduces into

$$\Delta W_{1/2} \approx \Delta F. \quad (\text{S12})$$

To estimate how much the work per step needs to exceed  $\Delta F$  in order for the ratio  $\pi_{\text{d}}/\pi_{\text{u}}$  to reach its saturation value of 1, we calculate the derivative of the ratio at  $\Delta W_{1/2} \approx \Delta F$ , namely,

$$\begin{aligned} \left. \frac{\partial}{\partial \Delta W} \left( \frac{\pi_{\text{d}}}{\pi_{\text{u}}} \right) \right|_{\Delta W_{1/2}} &= \frac{-\beta e^{-\beta(\Delta W_{1/2} + \Delta F)} (1 + e^{-\beta(\Delta W_{1/2} - \Delta F)}) + (1 + e^{-\beta(\Delta W_{1/2} + \Delta F)}) \beta e^{-\beta(\Delta W_{1/2} - \Delta F)}}{(1 + e^{-\beta(\Delta W_{1/2} - \Delta F)})^2} \\ &= \frac{\beta(1 - e^{-2\beta\Delta F})}{4} \\ &\approx \frac{1}{4k_{\text{B}}T}, \end{aligned} \quad (\text{S13})$$

where we again employed the  $e^{-2\beta\Delta F} \ll 1$  approximation. These results indicate that in order to overcome the equilibrium bias in piston state probabilities caused by the higher ligand entropy in the expanded state, the work per step needs to exceed the ligand free energy change upon compression ( $\Delta F$ ) by several  $k_{\text{B}}T$  values.

Now, we perform a similar set of calculations for the net rate of backward stepping ( $k_{\text{net}}$ ). Using its expression in eq 14, we obtain

$$k_{\text{net}} \Big|_{\Delta W_{1/2}} = \frac{(1 - e^{-2\beta\Delta W_{1/2}}) k_{\text{b}}}{1 + \cosh(\beta\Delta F) e^{-\beta\Delta W_{1/2}}} = \frac{k_{\text{b}}}{2} \quad (\text{S14})$$

Rearranging the terms, we obtain a quadratic equation for  $e^{\beta\Delta W_{1/2}}$ , namely,

$$e^{2\beta\Delta W_{1/2}} - \cosh(\beta\Delta F)e^{\beta\Delta W_{1/2}} - 2 = 0. \quad (\text{S15})$$

Since  $e^{\beta\Delta W_{1/2}} > 0$ , we take the positive solution and obtain

$$e^{\beta\Delta W_{1/2}} = \frac{\cosh(\beta\Delta F) + \sqrt{\cosh^2(\beta\Delta F) + 8}}{2}. \quad (\text{S16})$$

For large degrees of compression ( $e^{\beta\Delta F} \gg 1$ ), we can make the approximation  $\cosh(\beta\Delta F) \approx e^{\beta\Delta F}/2$  and ignore the constant term in the square root, which yields

$$e^{\beta\Delta W_{1/2}} \approx \frac{e^{\beta\Delta F}}{2}, \quad (\text{S17})$$

$$\Delta W_{1/2} \approx \Delta F - \beta^{-1} \ln 2. \quad (\text{S18})$$

Like in the treatment of the ratio  $\pi_d/\pi_u$ , we now estimate how much the work per step needs to exceed  $\Delta W_{1/2}$  in order for the backward stepping rate ( $k_{\text{net}}$ ) to reach its saturating value  $k_b$ . To that end, we calculate the derivative of  $k_{\text{net}}/k_b$  at  $\Delta W_{1/2}$ , namely,

$$\begin{aligned} \left. \frac{\partial}{\partial \Delta W} \left( \frac{k_{\text{net}}}{k_b} \right) \right|_{\Delta W_{1/2}} &= \frac{2\beta e^{-2\beta\Delta W_{1/2}}(1 + \cosh(\beta\Delta F)e^{-\beta\Delta W_{1/2}}) + (1 - e^{-2\beta\Delta W_{1/2}}) \cosh(\Delta F)\beta e^{-\beta\Delta W_{1/2}}}{(1 + \cosh(\beta\Delta F)e^{-\beta\Delta W_{1/2}})^2} \\ &\approx \frac{2\beta e^{-2\beta\Delta W_{1/2}}(1 + \frac{1}{2}e^{\beta\Delta F}e^{-\beta\Delta W_{1/2}}) + (1 - e^{-2\beta\Delta W_{1/2}})\frac{1}{2}e^{\beta\Delta F}\beta e^{-\beta\Delta W_{1/2}}}{(1 + \frac{1}{2}e^{\beta\Delta F}e^{-\beta\Delta W_{1/2}})^2} \\ &= \frac{4\beta e^{-2\beta\Delta W_{1/2}} + \beta(1 - e^{-2\beta\Delta W_{1/2}})}{4} \\ &\approx \frac{1}{4k_B T}. \end{aligned} \quad (\text{S19})$$

Here we made the approximation  $\cosh(\Delta F) \approx e^{\beta\Delta F}/2$  in the first step, used the result from eq S17 to write  $\frac{1}{2}e^{\beta\Delta F}e^{-\beta\Delta W_{1/2}} = 1$  in the second step, and in the last step ignored the  $e^{-2\beta\Delta W_{1/2}}$  terms since from eq S17 we have  $e^{-2\beta\Delta W_{1/2}} = 4e^{-2\beta\Delta F} \ll 1$  for large degrees of compression.

As we can see, when the work per step exceeds  $\Delta F$  by several  $k_B T$  values, the chances of forward stepping become vanishingly small compared with backward stepping, resulting in a net backward stepping rate  $k_{\text{net}} \approx k_b$ .

## C Equilibrium Properties of the Allosteric Enzyme

In this section, we introduce the constraints on the choices of rate constants for the enzyme stemming from the cycle condition (based on the fact that it does not consume energy), and also, discuss the fidelity available to it when the ligand concentration is held at a fixed value.

### C.1 Constraints on the Choice of Enzyme's Rate Constants

Consider the network of enzyme states and transitions in the absence of engine coupling redrawn in Figure S3A for convenience. Because the transitions between the states of the enzyme are not coupled to external energy consuming processes, the choice of the rate constants is constrained by the cycle condition which states that the products of rate constants in the clockwise and counterclockwise directions should be equal to each other in all the loops of the network diagram.<sup>3</sup> Imposing the cycle condition results in the constraint equations for the different loops shown in Figure S3B. In our analysis, we choose substrate unbinding to be the only process whose rate is different between right and wrong substrates ( $k_{\text{off}}^{\text{W}} > k_{\text{off}}^{\text{R}}$ ). Therefore, the rate constants of all other identical processes are chosen to be the same between the substrates, i.e.

$$k_{\text{A}}^{\text{R}} = k_{\text{A}}^{\text{W}} \equiv k_{\text{A}}^{\text{S}}, \quad (\text{S20})$$

$$k_{\text{I}}^{\text{R}} = k_{\text{I}}^{\text{W}} \equiv k_{\text{I}}^{\text{S}}, \quad (\text{S21})$$

$$k_{\text{A}}^{\text{R,L}} = k_{\text{A}}^{\text{W,L}} \equiv k_{\text{A}}^{\text{S,L}}, \quad (\text{S22})$$

$$k_{\text{I}}^{\text{R,L}} = k_{\text{I}}^{\text{W,L}} \equiv k_{\text{I}}^{\text{S,L}}, \quad (\text{S23})$$

where the superscript ‘‘S’’ stands for both right (‘‘R’’) and wrong (‘‘W’’) substrates. Using this general notation, we write the full set of constraint conditions on the rate constants obtained from the different loops (mid, front, and back) as

$$\text{mid: } \frac{k_{\text{I}}^{\text{L}}}{k_{\text{A}}^{\text{L}}} = \frac{\ell_{\text{off}}^{\text{A}}/\ell_{\text{on}}^{\text{A}}}{\ell_{\text{on}}^{\text{I}}/\ell_{\text{off}}^{\text{I}}} \frac{k_{\text{I}}}{k_{\text{A}}}, \quad (\text{S24})$$

$$\text{front: } \frac{k_{\text{I}}^{\text{S}}}{k_{\text{A}}^{\text{S}}} = \frac{k_{\text{on}}^{\text{I}}}{k_{\text{on}}^{\text{A}}} \frac{k_{\text{I}}}{k_{\text{A}}}, \quad (\text{S25})$$

$$\text{back: } \frac{k_{\text{I}}^{\text{S,L}}}{k_{\text{A}}^{\text{S,L}}} = \frac{k_{\text{on}}^{\text{I}}}{k_{\text{on}}^{\text{A}}} \frac{k_{\text{I}}^{\text{L}}}{k_{\text{A}}^{\text{L}}}. \quad (\text{S26})$$

Note that the conditions imposed on the side loops follow directly from those of the other three loops via

$$\text{side} = \frac{\text{mid} \times \text{back}}{\text{front}}, \quad (\text{S27})$$

which is why the side loops do not contribute a unique condition.

When writing the cycle conditions we did not include the product formation rate constant  $r$ , despite the fact that production takes the enzyme into its substrate-free state, just like what unbinding through  $k_{\text{off}}$  reactions does. The reason for this is that  $r$  is an effective rate

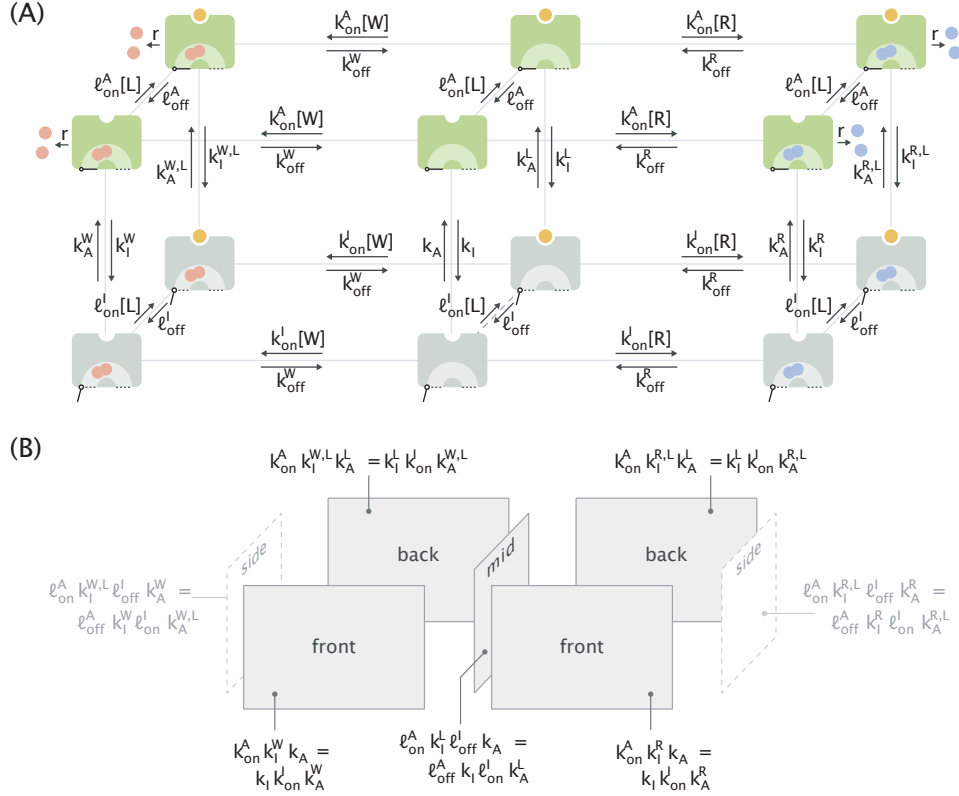


**Figure S3.** The allosteric enzyme in the absence of engine coupling. (A) Network diagram of enzyme states and transitions between them at a fixed ligand concentration. The diagram is redrawn identically from Figure 4 for convenience. (B) Cycle condition on rate constants applied for the different loops of the diagram. The lighter color of the side loop conditions indicates that they are redundant and follow from the conditions on the other three loops.

constant for the process  $E : S \xrightarrow{r} E + P$  representing the coarse-grained version of the full biochemical pathway of enzymatic production, namely,  $E : S \rightleftharpoons E : P \rightleftharpoons E + P$ , which is distinct from the  $k_{off}$  pathway of emptying the enzyme. In our treatment we assume that product formation is practically irreversible which will be true if the product concentration is kept low and, optionally, if the reverse reaction  $P \longrightarrow S$  is energetically highly unfavorable (e.g. requires a spontaneous formation of a covalent bond).

If the product formation rate is nonzero ( $r > 0$ ), the enzyme will be out of equilibrium despite the fact that its individual transitions are not coupled to an energy source. This is due to the implicit assumption of having the right and wrong substrate concentrations fixed, which makes the system open (i.e. new substrates enter and products exit the system). We discuss the implications of this open system feature on the fidelity of the enzyme in the absence of driving in the next section.

## C.2 Enzyme Fidelity at a Fixed Ligand Concentration

As mentioned in the previous section, the presence of a nonzero production rate ( $r > 0$ ) makes the system open and thereby takes the enzyme out of equilibrium even at a fixed ligand concentration where the engine-enzyme coupling is absent. For Hopfield's scheme, it can be shown that in an analogous situation where driving is absent but the system is open, the "equilibrium" (un-driven) fidelity is confined in a range defined by the ratio of the Michaelis and dissociation constants, which, for equal on-rates ( $k_{\text{on}}^{\text{R}} = k_{\text{on}}^{\text{W}}$ ), becomes

$$\eta_{\text{eq}} \in \left[ \frac{k_{\text{off}}^{\text{W}} + r}{k_{\text{off}}^{\text{R}} + r}, \frac{k_{\text{off}}^{\text{W}}}{k_{\text{off}}^{\text{R}}} \right]. \quad (\text{S28})$$

We hypothesize that the same holds true for the allosteric enzyme as well despite the much wider diversity of states available to it. To demonstrate that, we first consider the limiting  $r \rightarrow 0$  case where the product formation is so slow that the system effectively exists in a thermodynamic equilibrium. All possible enzyme states along with their statistical weights in this equilibrium setting are shown in Figure S4. Fidelity can be found by adding the statistical weights of the right and wrong substrate-bound active states and dividing them, yielding

$$\eta_{\text{eq}}(r \rightarrow 0) = \frac{[\text{R}]}{[\text{W}]} \frac{K_{\text{D}}^{\text{W,A}}}{K_{\text{D}}^{\text{R,A}}} = \frac{k_{\text{off}}^{\text{W}}}{k_{\text{off}}^{\text{R}}}, \quad (\text{S29})$$

where we used  $[\text{R}] = [\text{W}]$  and the equal on-rate assumption to go from dissociation constants to unbinding rates. This corresponds to the upper limit in eq S28.

state	weight	state	weight	state	weight
	$\frac{[\text{W}]}{K_{\text{D}}^{\text{W,A}}} e^{-\epsilon_{\text{A}}}$		$e^{-\epsilon_{\text{A}}}$		$\frac{[\text{R}]}{K_{\text{D}}^{\text{R,A}}} e^{-\epsilon_{\text{A}}}$
	$\frac{[\text{W}]}{K_{\text{D}}^{\text{W,I}}} e^{-\epsilon_{\text{I}}}$		$e^{-\epsilon_{\text{I}}}$		$\frac{[\text{R}]}{K_{\text{D}}^{\text{R,I}}} e^{-\epsilon_{\text{I}}}$
	$\frac{[\text{L}]}{R_{\text{D}}^{\text{A}}} \frac{[\text{W}]}{K_{\text{D}}^{\text{W,A}}} e^{-\epsilon_{\text{A}}}$		$\frac{[\text{L}]}{R_{\text{D}}^{\text{A}}} e^{-\epsilon_{\text{A}}}$		$\frac{[\text{L}]}{R_{\text{D}}^{\text{A}}} \frac{[\text{R}]}{K_{\text{D}}^{\text{R,A}}} e^{-\epsilon_{\text{A}}}$
	$\frac{[\text{L}]}{R_{\text{D}}^{\text{I}}} \frac{[\text{W}]}{K_{\text{D}}^{\text{W,I}}} e^{-\epsilon_{\text{I}}}$		$\frac{[\text{L}]}{R_{\text{D}}^{\text{I}}} e^{-\epsilon_{\text{I}}}$		$\frac{[\text{L}]}{R_{\text{D}}^{\text{I}}} \frac{[\text{R}]}{K_{\text{D}}^{\text{R,I}}} e^{-\epsilon_{\text{I}}}$
$\left(1 + \frac{[\text{L}]}{R_{\text{D}}^{\text{A}}}\right) \frac{[\text{W}]}{K_{\text{D}}^{\text{W,A}}} e^{-\epsilon_{\text{A}}}$				$\left(1 + \frac{[\text{L}]}{R_{\text{D}}^{\text{A}}}\right) \frac{[\text{R}]}{K_{\text{D}}^{\text{R,A}}} e^{-\epsilon_{\text{A}}}$	

**Figure S4.** Table of possible enzyme states and their statistical weights in the  $r \rightarrow 0$  limit where the system is effectively at equilibrium. Here  $\epsilon_{\text{A}}$  and  $\epsilon_{\text{I}}$  stand for the energies of the enzyme in its active and inactive states, respectively. The dissociation constants of the ligand and the substrates are denoted by  $R_{\text{D}}$  and  $K_{\text{D}}$ , respectively.

Intuitively, the presence of a nonzero production rate ( $r > 0$ ) should reduce the fidelity

since the enzyme would have less time to perform substrate filtering in its active state before product formation takes place. To study how large this reduction can be, let us first consider a limiting case where the enzyme is exclusively in its active state – a setting where we expect the reduction effect to be manifested the most. The active “slice” of the full network diagram corresponding to this limiting case is depicted in Figure S5A. Since product formation is just another path to substrate unbinding, we can derive a corresponding reduced network diagram by adding the production rate to the off-rates, as shown in Figure S5B.

A peculiar feature of this network is that the cycle condition holds in its two loops, despite the fact that the system is open ( $r > 0$ ). This means that at steady state the detailed balance condition will hold on all edges of the network (cf. Schnakenberg,<sup>4</sup> section X), allowing us to assign effective statistical mechanical weights to the different states (Figure S5C).

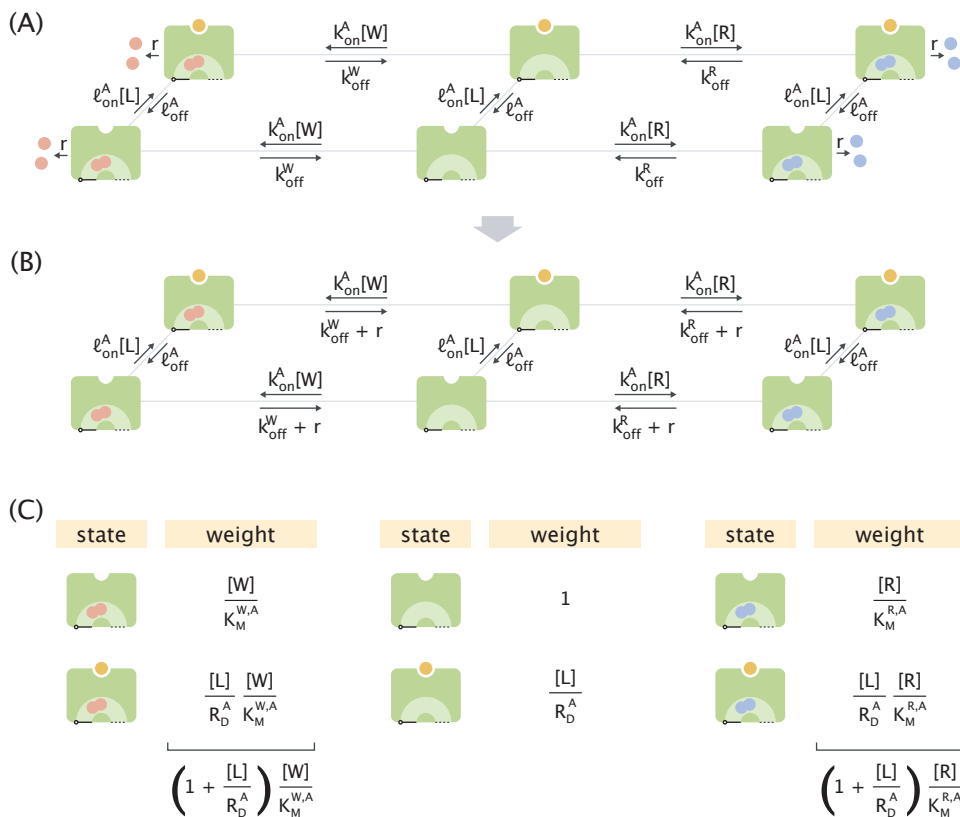


**Figure S5.** The enzyme in the limit of constant activity and in the absence of engine coupling. (A) The active “slice” of the enzyme’s full network diagram depicted in Figure S3A. (B) The reduced diagram corresponding to the network in panel A with the production and off-rates combined under the same reaction arrow. (C) Table of the different enzyme states and their effective statistical weights.  $K_M$  stands for the Michaelis constant. Total weights of the wrong and right substrate-bound states are shown below the left and right columns, respectively.

Dividing the total weights of the right and wrong substrate-bound states, we obtain the

fidelity in this special limit where the enzyme is exclusively in its active state, namely,

$$\eta_{\text{eq}}^{\text{active}}(r > 0) = \frac{[\text{R}]}{[\text{W}]} \frac{K_{\text{M}}^{\text{W,A}}}{K_{\text{M}}^{\text{R,A}}} = \frac{k_{\text{off}}^{\text{W}} + r}{k_{\text{off}}^{\text{R}} + r}. \quad (\text{S30})$$

Here we again used  $[\text{R}] = [\text{W}]$  and the equal on-rate assumption. Note that this corresponds to the lower fidelity limit in the un-driven Hopfield model (eq. S28).

We now hypothesize that the enzyme’s fidelity falls between these two limits in the general case where the system is open ( $r > 0$ ) and when the states are not constrained to be in the active “slice” of the full network diagram. Since obtaining the exact expression of fidelity in the general case is highly complicated due to the presence of a large number of states and loops in the network diagram, and since a paper-and-pencil approach where the symmetries existing between the left and right “wings” of the network could potentially be taken advantage of to provide an analytical proof is also not straightforward, we use a numerical method instead to justify our hypothesis.

To that end, we fixed the ratio of the wrong and right substrate off-rates to be  $k_{\text{off}}^{\text{W}}/k_{\text{off}}^{\text{R}} = 100$ , sampled values for enzyme’s remaining transition rate constants from the  $[10^{-4}k_{\text{off}}^{\text{R}}, 10^4k_{\text{off}}^{\text{R}}]$  range (generating 20,971,520 independent sets in total), and evaluated the fidelity for each parameter set. The results of the numerical study are summarized in Figure S6. As can be seen, despite the wider diversity of allosteric enzyme’s states, its fidelity in the absence of engine coupling still falls between the “equilibrium” limits of Hopfield’s model (eq S28).

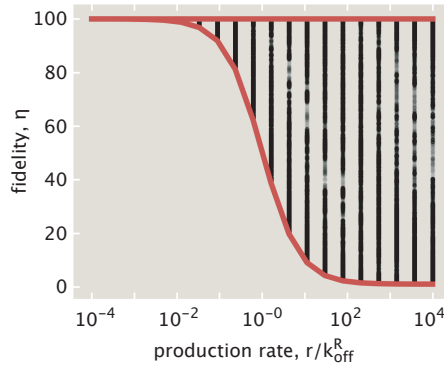


**Figure S6.** Allosteric enzyme’s fidelity in the absence of engine coupling (fixed  $[\text{L}]$ ) for different choices of transition rates. The upper and lower red curves correspond to the ratios of the dissociation (eq S29) and Michaelis constants (eq S30), respectively. Only the data points with fidelity values different up to the third significant digit were used in the plot.

# D Full Description of the Piston Model with Engine-Enzyme Coupling

In this section, we provide details on the analytical and numerical explorations of the full model. In D.1 we discuss the thermodynamics of coupling the engine to the allosteric enzyme. Then, in D.2 we present the methodology for obtaining the steady state probabilities of system states under external drive. In D.3 and D.4 we provide the parameters used in the numerical study of section 3.3 and describe the fidelity optimization strategy used in study of the section 3.4, respectively. Lastly, in D.5 we investigate in detail the  $\alpha_{\max} \approx 3$  result for the highest fidelity of the model.

## D.1 Equilibrium Fidelity of the Piston Model in the Absence of External Driving

In Supporting Information section C.2 we showed that at a fixed ligand concentration the fidelity of the allosteric enzyme was constrained within the range given in eq S28. Here we demonstrate that the same result holds also for the full model in the absence of external driving when a thermodynamically consistent coupling is made between the engine and the enzyme.

In the absence of driving, the finite-state equivalent of the full network (Figure 5D) can be reduced into the one shown in Figure S7 where we have combined the ratchet transitions through forward and backward pathways under a single arrow – a procedure allowed when the transitions are not driven.<sup>5</sup> Because of the equilibrium constraints imposed on the enzyme’s transition rates discussed in Supporting Information section C.1, the cycle condition will hold for the loops in the left and right “layers” of the diagram in Figure S7. The loops where the cycle condition could possibly be violated are the ones that involve transitions between the two layers, i.e. piston compressions and expansions.

The first class of such loops does not involve ligand binding and unbinding events (for example, the shaded vertical rectangle in Figure S7) and therefore, the cycle condition is automatically satisfied in such loops since for each clockwise transition there is a corresponding counterclockwise transition with an identical rate. The second class of loops that connect the two layers involves ligand binding and unbinding events which affect the rate of switching between the layers (e.g. the shaded horizontal rectangle in Figure S7). The driving force in these loops is given by

$$\Delta\mu = \beta^{-1} \ln \frac{(k_f^{u \rightarrow d} + k_b)(k_f^{d \rightarrow u, L} + k_b)[L]_d}{(k_f^{d \rightarrow u} + k_b)(k_f^{u \rightarrow d, L} + k_b)[L]_u}, \quad (\text{S31})$$

where we used the fact that the ligand binding rates are proportional to ligand concentrations. Now, in the general case where there are  $N$  ligands under the piston (one of which can be bound to the enzyme), the different forward stepping rates become

$$k_f^{u \rightarrow d} = k_b e^{-\beta(\Delta W_{\text{eq}} + \beta^{-1} N \ln f)} = k_b f^{-N}, \quad (\text{S32})$$

$$k_f^{u \rightarrow d, L} = k_b e^{-\beta(\Delta W_{\text{eq}} + \beta^{-1} (N-1) \ln f)} = k_b f^{-(N-1)}, \quad (\text{S33})$$

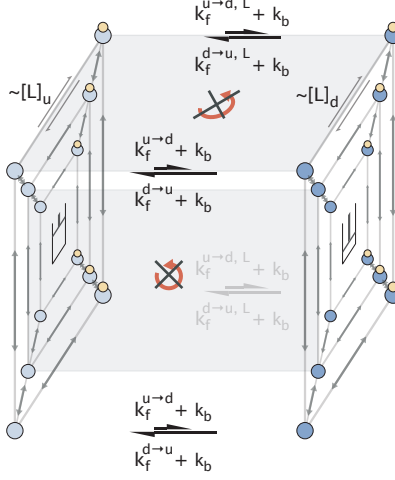


**Figure S7.** The effective network diagram of the piston model in the absence of driving. The forward and backward pathways connecting the two layers of the diagram are combined to yield effective rates. The two kinds of cycles where ligand binding events are present or absent are shown as horizontal and vertical shaded rectangles, respectively. The crossed cycling arrows indicate the absence of driving forces in the shaded loops.

$$k_f^{d \rightarrow u} = k_b e^{-\beta(\Delta W_{\text{eq}} - \beta^{-1} N \ln f)} = k_b f^N, \quad (\text{S34})$$

$$k_f^{d \rightarrow u, L} = k_b e^{-\beta(\Delta W_{\text{eq}} - \beta^{-1} (N-1) \ln f)} = k_b f^{N-1}. \quad (\text{S35})$$

Here we set  $\Delta W_{\text{eq}} = 0$  to account for the absence of driving and used the fact that the free energy change of  $N$  ligands upon isothermal compression is  $\beta^{-1} N \ln f$  (with a negative sign upon expansion) and that  $N$  should be replaced with  $N - 1$  when one of the ligands is bound to the enzyme.

Substituting these expressions into eq S31 and using the identity  $[L]_d = f[L]_u$ , we find

$$\begin{aligned} \Delta\mu &= \beta^{-1} \ln \frac{(f^{-N} + 1)(f^{N-1} + 1)f}{(f^N + 1)(f^{1-N} + 1)} \\ &= \beta^{-1} \ln \left( \frac{f^{-N}(1 + f^N)}{f^N + 1} \times \frac{f^{N-1}(1 + f^{1-N})}{f^{1-N} + 1} \times f \right) \\ &= \beta^{-1} \ln (f^{-N} \times f^{N-1} \times f) \\ &= \beta^{-1} \ln 1 = 0. \end{aligned} \quad (\text{S36})$$

This shows that in the absence of external driving ( $\Delta W = 0$ ) the cycle condition holds for all loops of the network, demonstrating the thermodynamic consistency of the coupling between the engine and the enzyme.

As in our separate treatment of the allosteric enzyme in Supporting Information section C.2, here too in the  $r \rightarrow 0$  limit the system will approach a thermodynamic equilibrium. Since we already know that in the equilibrium limit the fidelity of the enzyme at a fixed ligand concentration is given by the ratio of the wrong and right off-rates, we can apply this result to the left and right layers of the diagram in Figure S7 and obtain a relation between

the net statistical weights of the right and wrong substrate-bound active states, namely,

$$\frac{w_u^R}{w_u^W} = \frac{w_d^R}{w_d^W} = \frac{k_{\text{off}}^W}{k_{\text{off}}^R}. \quad (\text{S37})$$

Here “u” and “d” stand for the expanded (left layer) and compressed (right layer) states of the piston. We can then write the fidelity of the full network in terms of these weights as

$$\eta_{\text{eq}}(r \rightarrow 0) = \frac{w_u^R + w_d^R}{w_u^W + w_d^W} = \frac{w_u^W \left( \frac{k_{\text{off}}^W}{k_{\text{off}}^R} \right) + w_d^W \left( \frac{k_{\text{off}}^W}{k_{\text{off}}^R} \right)}{w_u^W + w_d^W} = \frac{k_{\text{off}}^W}{k_{\text{off}}^R}, \quad (\text{S38})$$

which corresponds to the upper limit of the equilibrium fidelity range in eq S28.

To demonstrate that in the absence of driving the coupled system meets also the lower fidelity limit given by  $(k_{\text{off}}^W + r)/(k_{\text{off}}^R + r)$ , we again use a numerical approach and sample the parameter space, evaluating the fidelity at each of the 10,628,820 sampled sets of parameters. As in the study of Figure S7, here too we set the ratio of off-rates to be  $k_{\text{off}}^W/k_{\text{off}}^R = 100$ . The results are summarized in Figure S8, where it can be seen that all points lie between the limits of eq S28. Overall, this study shows that in the absence of driving, the coupling of the engine to the enzyme alone cannot lead to fidelity enhancement.

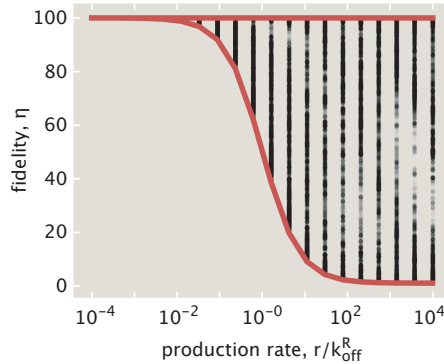


**Figure S8.** Fidelity of the full piston model in the absence of driving ( $\Delta W = 0$ ) for different choices of model parameters. The upper and lower red curves correspond to the ratios of the dissociation (eq S29) and Michaelis constants (eq S30), respectively. Only the data points with fidelity values different up to the third significant digit were used in the plot.

## D.2 Obtaining the Steady-State Occupancy Probabilities

The kinetics of the full piston model is characterized by a  $24 \times 24$  transition rate matrix  $\mathbf{Q}$ , which has the block form

$$\mathbf{Q} = \begin{pmatrix} \mathbf{Q}_u^{\text{enzyme}} & \mathbf{Q}_{d \rightarrow u} \\ \mathbf{Q}_{u \rightarrow d} & \mathbf{Q}_d^{\text{enzyme}} \end{pmatrix}. \quad (\text{S39})$$

Here the non-diagonal elements of the  $12 \times 12$  matrices  $\mathbf{Q}_u^{\text{enzyme}}$  and  $\mathbf{Q}_d^{\text{enzyme}}$  represent the transition rates between the different enzyme states when the ligand concentration is  $[L] = [L]_u$  and  $[L] = [L]_d$ , respectively. These non-diagonal terms at a given ligand concentration  $[L]$  are depicted in Figure S9.

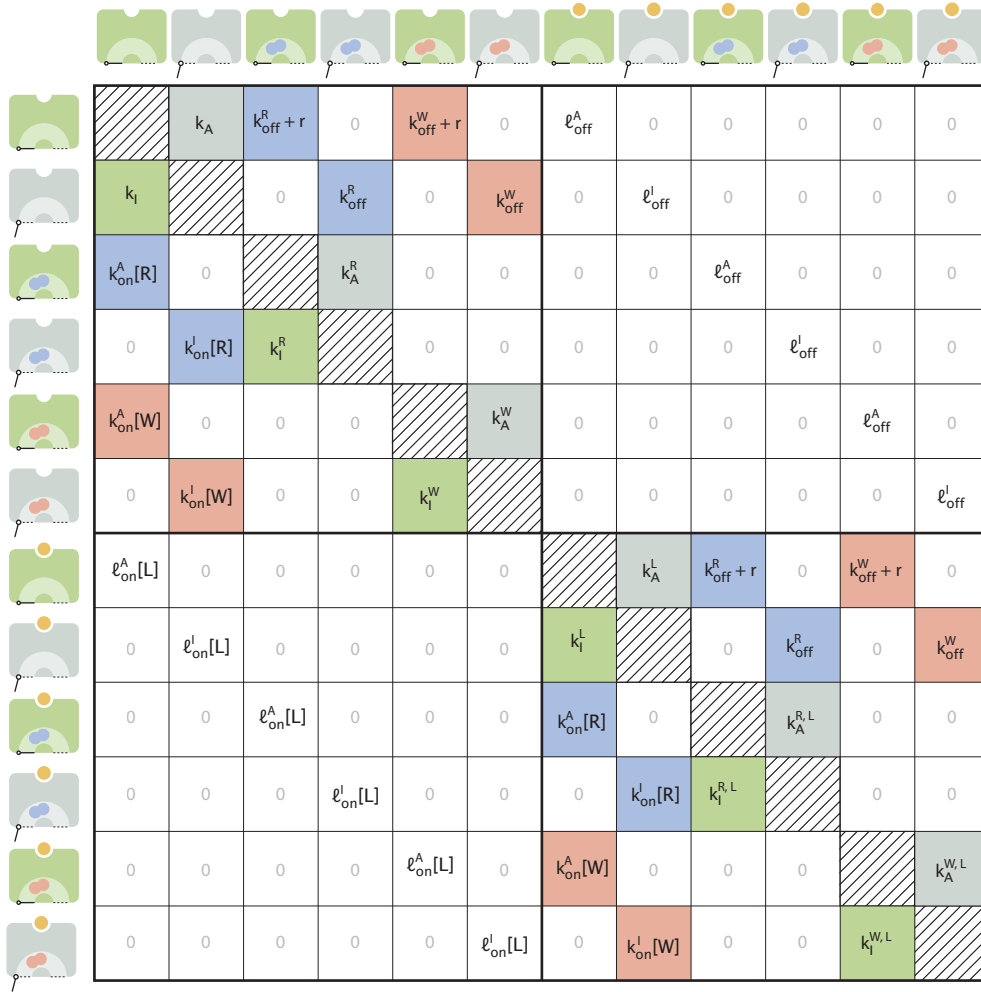


**Figure S9.** Transition rates between the enzyme states. The element  $Q_{i,j}^{\text{enzyme}}$  stands for the rate of transitioning from the  $j^{\text{th}}$  into the  $i^{\text{th}}$  state of the enzyme ( $i \neq j$ ) at a fixed ligand concentration  $[L]$ . Red- and blue-colored cells show transitions involving the binding or release of incorrect and correct substrates, respectively. Green- and gray-colored cells show inactivating and activating enzyme transitions, respectively. The diagonals are shaded to indicate that they are not used when constructing  $\mathbf{Q}$ .

The other two matrices, namely,  $\mathbf{Q}_{d \rightarrow u}$  and  $\mathbf{Q}_{u \rightarrow d}$ , are diagonal whose elements stand for the net piston compression ( $d \rightarrow u$ ) and expansion ( $u \rightarrow d$ ) rates that alter the state of the piston but leave the state of the enzyme unchanged. They are given by

$$\mathbf{Q}_{d \rightarrow u} = \text{diag} \left( \underbrace{(k_b + k_f^{d \rightarrow u}), \dots, (k_b + k_f^{d \rightarrow u})}_{6 \text{ terms}}, \underbrace{(k_b + k_f^{d \rightarrow u, L}), \dots, (k_b + k_f^{d \rightarrow u, L})}_{6 \text{ terms}} \right), \quad (\text{S40})$$

$$\mathbf{Q}_{u \rightarrow d} = \text{diag} \left( \underbrace{(k_b + k_f^{u \rightarrow d}), \dots, (k_b + k_f^{u \rightarrow d})}_{6 \text{ terms}}, \underbrace{(k_b + k_f^{u \rightarrow d, L}), \dots, (k_b + k_f^{u \rightarrow d, L})}_{6 \text{ terms}} \right). \quad (\text{S41})$$

Note that since the forward stepping rates depend on whether the ligand is bound or not, they appear without a superscript ‘‘L’’ in the first 6 terms (where the ligand unbound), and with a superscript ‘‘L’’ in the last 6 terms (where the ligand is bound). Lastly, the diagonal elements of  $\mathbf{Q}$  are assigned such that  $Q_{jj} = -\sum_{i \neq j} Q_{ij}$ , ensuring that the columns sum to zero.

The dynamics of the coupled engine-enzyme system is described via

$$\frac{d\vec{p}}{dt} = \mathbf{Q}\vec{p}, \quad (\text{S42})$$

where  $\vec{p}$  is a column vector whose 24 elements stand for the probabilities of the different system states (12 enzyme states  $\times$  2 piston states). We are interested in the steady state behavior of the piston model, where  $d\vec{p}/dt = \vec{0}$ . Since the exact analytical expressions for the steady state probabilities  $\vec{p}_{\text{ss}} \equiv \vec{\pi}$  are highly convoluted, in our parametric studies we use numerical methods to find  $\vec{\pi}$  from  $\mathbf{Q}\vec{\pi} = \vec{0}$  and  $\sum_i \pi_i = 1$ , where the latter equation guarantees that the probabilities sum to 1.

### D.3 Enzyme’s Kinetic Parameters Used for the Numerical Study in Section 3.4

Here we provide the list of enzyme’s transition rates used for numerically studying the effects of tuning the engine “knobs” in section 3.4. Since none of the performance metrics used in the study depend on the absolute timescale of the model’s dynamics, we set the unbinding rate of the right substrate to be unity ( $k_{\text{off}}^{\text{R}} = 1$ ), and defined all other rates relative to it. Specifically, we chose  $k_{\text{off}}^{\text{W}} = 100$  so that the fidelity after a single proofreading realization roughly matched that of the ribosome ( $\eta_{\text{translation}} \sim 10^4$ ).<sup>6</sup> Also, we chose the catalysis rate to be much slower compared with the off-rates ( $r = 0.2$ ) - a condition for high fidelity suggested in Hopfield’s original paper.

The remaining rate constants were assigned values that meet the intuitive expectations from the conceptual introduction of the model in section 2. Specifically, the rate of substrate binding to the active enzyme was chosen to be much less than the rate of binding to the inactive enzyme in order to yield low leakiness ( $k_{\text{on}}^{\text{A}}/k_{\text{on}}^{\text{I}} = 10^{-5} \ll 1$ ). Next, the enzyme was chosen to be predominantly inactive in its native state to allow for new substrate binding events ( $k_{\text{I}}/k_{\text{A}} = 50 \gg 1$ ). Lastly, the rates of ligand binding and unbinding were assigned values that ensure that the ligand acts as a strong activator ( $\frac{\ell_{\text{off}}^{\text{I}}/\ell_{\text{on}}^{\text{I}}}{\ell_{\text{off}}^{\text{A}}/\ell_{\text{on}}^{\text{A}}} = 10^6 \gg 1$ ).

The values of the independent parameters  $k_{\text{A}}^{\text{L}}$  and  $k_{\text{A}}^{\text{S}}$  were assigned after manually inspecting the effect of different numerical choices on the model performance. Finally, the values of the remaining four parameters (lower section in Table S1) were calculated from the cycle conditions in eqs S24-S26 under the assumption that ligand binding does not alter the ratio of inactivation or activation rates in the substrate-bound and substrate-unbound states (i.e.  $k_{\text{I}}^{\text{S,L}}/k_{\text{I}}^{\text{L}} = k_{\text{I}}^{\text{S}}/k_{\text{I}}$  and  $k_{\text{A}}^{\text{S,L}}/k_{\text{A}}^{\text{L}} = k_{\text{A}}^{\text{S}}/k_{\text{A}}$ ).

**Table S1.** Values of enzyme’s different transition rates used in the studies of Figure 6.

Transition rate	Value
$k_{\text{off}}^{\text{R}}, k_{\text{off}}^{\text{W}}$	1, 100
$r$	0.2
$k_{\text{on}}^{\text{A}} [\text{S}]$	$10^{-5}$
$k_{\text{on}}^{\text{I}} [\text{S}]$	1
$k_{\text{A}}$	20
$k_{\text{I}}$	1000
$\ell_{\text{on}}^{\text{A}}$	0.1
$\ell_{\text{off}}^{\text{A}}$	5
$\ell_{\text{on}}^{\text{I}}$	0.01
$\ell_{\text{off}}^{\text{I}}$	500000
$k_{\text{A}}^{\text{L}}$	2000
$k_{\text{A}}^{\text{S}}$	0.01
$k_{\text{I}}^{\text{L}}$	0.1
$k_{\text{I}}^{\text{S}}$	50000
$k_{\text{A}}^{\text{S,L}}$	1
$k_{\text{I}}^{\text{S,L}}$	5

## D.4 Details of the Numerical Optimization Procedure for Finding the Highest Fidelity

In our optimization scheme, we first chose the values of rates which were kept fixed for the rest of the study. These include the unbinding rate of right substrates ( $k_{\text{off}}^{\text{R}} = 1$ ), the catalysis rate ( $r = 0.2$ ), and the effective first-order rate of substrate binding to the inactive enzyme state ( $k_{\text{on}}^{\text{I}}[\text{S}] = 1$ ). Also, since no limits were imposed on the amount of energy expenditure, we chose large values for the compression factor ( $f = 10^{100}$ ) and the work per step ( $\Delta W = 1000 k_{\text{B}}T$ ) to maximize the quality of proofreading.

Then, we considered a set of 144 different initialization options for the remaining parameters to be used in our numerical optimization procedure. To avoid the completely independent tuning of related enzyme activation and inactivation rates, we considered three possible options that met the cycle condition. Namely, 1)  $k_{\text{A}}^{\text{S}} = k_{\text{A}}$  and  $k_{\text{I}}^{\text{S}} = k_{\text{I}}/\gamma$ , 2)  $k_{\text{A}}^{\text{S}} = \sqrt{\gamma}k_{\text{A}}$  and  $k_{\text{I}}^{\text{S}} = k_{\text{I}}/\sqrt{\gamma}$ , 3)  $k_{\text{A}}^{\text{S}} = \gamma k_{\text{A}}$  and  $k_{\text{I}}^{\text{S}} = k_{\text{I}}$ , where  $\gamma = k_{\text{on}}^{\text{A}}/k_{\text{on}}^{\text{I}}$ . All of these three options satisfy the cycle constraint  $k_{\text{on}}^{\text{A}}k_{\text{I}}^{\text{S}}k_{\text{A}} = k_{\text{on}}^{\text{I}}k_{\text{A}}^{\text{S}}k_{\text{I}}$  (Figure S3B). Options for the transition rates between ligand-bound enzyme states (i.e.  $k_{\text{A}}^{\text{S,L}}$  and  $k_{\text{I}}^{\text{S,L}}$ ) were chosen analogously.

In our custom-written maximization algorithm we iteratively perturbed all the parameters for multiple rounds with decreasing amplitudes until the convergence criterion was met or until the number of iterations exceeded the specified threshold (at most 20 iterations for each of the 6 decreasing amplitudes). The results from each of these local maximization procedures are summarized in Figure S10. We chose the largest among the different local maxima to represent the highest fidelity available for the given  $(k_{\text{on}}^{\text{A}}, k_{\text{off}}^{\text{W}})$  pair.

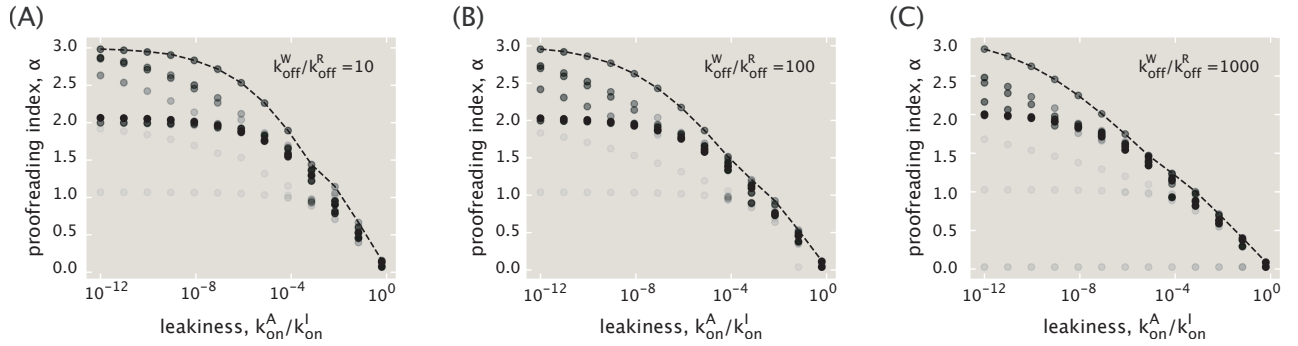


**Figure S10.** Fidelity optimization results for each of the 144 parameter initialization options. (A)  $k_{\text{off}}^{\text{W}}/k_{\text{off}}^{\text{R}} = 10$ . (B)  $k_{\text{off}}^{\text{W}}/k_{\text{off}}^{\text{R}} = 100$ . (C)  $k_{\text{off}}^{\text{W}}/k_{\text{off}}^{\text{R}} = 1000$ . The dotted lines in each panel represent the trends for the globally optimal fidelities.

## D.5 Investigation of the $\alpha_{\max} \approx 3$ Result for the Highest Available Proofreading Index

Our numerical scheme for optimizing the fidelity (Supporting Information section D.4) revealed that the piston model could perform proofreading up to three times ( $\alpha_{\max} \approx 3$ ). To gain intuition on how this is possible, let us consider the wrong “wing” of the full reaction network (Figure S11A). Each system state is characterized by the piston position (up or down) and the state of the enzyme (one of 8 possibilities). To turn a wrong substrate into a product, the system needs to traverse a trajectory that starts at a substrate-unbound state on the right side of the diagram and reaches one of the substrate-bound active states on the left side, at which point catalysis can take place. Using the terminology introduced in Murugan, *et al.*,<sup>7</sup> we can say that a proofreading filter can be realized every time the system makes a transition parallel to the “discriminatory fence” of the network (Figure S11A). Rates which are on either side of the fence do not discriminate between the two kinds of substrates; only those that cross the fence do, which in our case are the off-rates ( $k_{\text{off}}^{\text{W}} > k_{\text{off}}^{\text{R}}$ ). Thus, the number of such parallel transitions that the system makes before reaching the catalytically active state represents the largest number of proofreading filters available to the given trajectory.

Figure S11B shows the full list of unique trajectories that start on the right side of the network, cross the discriminatory fence and eventually reach an active enzyme state after traversing through a series of inactive states. The trajectories are grouped by the number of these inactive states visited on the left side of the wing prior to reaching the active state. For example, entries of the first group represent trajectories where the substrate binds directly to the active enzyme and hence, undergoes zero proofreading filtrations. The discriminatory capacity of the piston model will therefore depend on which of the trajectories dominates in product formation.

To compare the contributions from different trajectories, we assign each of them a probability flux, which approximates the average rate of product formation through the trajectory. We define this flux via

$$J_{\vec{s}} = \pi_{s_0} k_{s_0 \rightarrow s_1} \left( \prod_{i=1}^{N-2} p_{s_i \rightarrow s_{i+1}} \right) p_{s_{N-1}}^{\text{cat}}, \quad (\text{S43})$$

where  $\vec{s}$  is the set of  $N$  states in the trajectory,  $\pi_{s_0} k_{s_0 \rightarrow s_1}$  is the substrate binding flux that crosses the fence at the start of the trajectory,  $p_{s_i, s_{i+1}}$  are the probabilities of staying on the trajectory during traversal, and, lastly,  $p_{s_{N-1}}^{\text{cat}}$  is the probability of catalysis once the system has reached the active enzyme state  $s_{N-1}$ . Note that the flux expression does not account for backtracking events whose contribution we expect to be insignificant for efficient proofreading trajectories, since for them  $p_{s_i \rightarrow s_{i+1}} \ll 1$ .

Having defined a flux metric for each trajectory, we then calculated its value for all trajectories listed in Figure S11B in the case where  $k_{\text{off}}^{\text{W}}/k_{\text{off}}^{\text{R}} = 100$  and  $k_{\text{on}}^{\text{A}}/k_{\text{on}}^{\text{I}} = 10^{-12}$  (low leakiness). Figure S11C shows the fluxes normalized by the highest one and grouped by the number of proofreading filters. As we can see, the dominant trajectory indeed contains three filters. This dominant trajectory is highlighted in red in Figure S11B and also corresponds to the one shown in Figure 7B of the main text.



**Figure S11.** (A) The wrong “wing” of the full reaction network along with the discriminatory fence. Ligand concentrations that enter the ligand binding rates are shown to indicate the difference between the upper and lower halves of the diagram. (B) The full set of unique trajectories that start on the right side of the network and end up at an active enzyme state on the left side. Numbers of proofreading filters available to trajectories are shown on the side. Piston state transitions are marked with dotted lines for clarity. The dominant trajectory in panel (C) is highlighted in red. (C) The relative product formation fluxes of all possible trajectories calculated for the case where  $k_{\text{off}}^W/k_{\text{off}}^R = 100$  and  $k_{\text{on}}^A/k_{\text{on}}^I = 10^{-12}$ , and grouped by the number of filters. The red dot indicates the dominant one. (D) Schematic illustration of the dominant trajectory in panel (C) along with the numerical values of the rates. The dotted arrows suggest that the intermediate transitions are much slower than the off-rate.

We would like to note here that the model parameters inferred from the unconstrained fidelity optimization were degenerate, and there was an alternative set with  $\alpha \approx 3$  proofreading index whose corresponding dominant trajectory was different from the one highlighted in Figure S11B. Some of the parameters of this set, however, contradicted our model criteria (e.g. the binding rate in the expanded piston state was very high), which is why we did not use this alternative set for our main discussion. Parameters that did satisfy our model criteria are shown for the  $k_{\text{off}}^{\text{W}}/k_{\text{off}}^{\text{R}} = 100$  case in Figure S11D. The transition rates between intermediates are much slower compared with the off-rate, as expected for an efficient proofreading performance.

Lastly, as can be seen in Figure S11B, the highest number of filters that a unique trajectory could, in principle, realize is 4 and not 3. This raises the question of why a trajectory with 4 potential filters cannot be a dominant one, as our numerical results in Figure S11C have suggested. We answer this question for three representative cases and invite the reader to work through the remaining examples. Our approach will be to show that the flux through a given 4-filter trajectory is necessarily less than that of some other trajectory with fewer filters, which would suggest that it cannot be a dominant one.

Figure S12 shows three different 4-filter trajectories next to corresponding trajectories with fewer filters, flux through which, as we will show, will necessarily be greater. Throughout our analysis we will be making use of the fact that the rates of piston expansion and compression are identical (and equal to  $k_{\text{b}}$ ) in the large driving limit considered here. Let us start from the first example. Using Eq S43, we can write the fluxes through 4-filter ( $J_{(4)}$ ) and 3-filter ( $J_{(3)}$ ) trajectories respectively as

$$J_{(4)} = \pi_0 k_{0 \rightarrow 1} \times p_{1 \rightarrow 2} p_{2 \rightarrow 3} p_{3 \rightarrow 4} p_{4 \rightarrow 5} \times p_5^{\text{cat}}, \quad (\text{S44})$$

$$J_{(3)} = \pi_0 k_{0 \rightarrow 1} \times p_{1 \rightarrow 2} p_{2 \rightarrow 3} p_{3 \rightarrow 6} \times p_6^{\text{cat}}. \quad (\text{S45})$$

Since the states (3) and (4) correspond to the same enzyme state and have identical outgoing rates, we have  $p_{4 \rightarrow 5} = p_{3 \rightarrow 6}$ . From the same argument for states (5) and (6) we find  $p_5^{\text{cat}} = p_6^{\text{cat}}$ . With these identities at hand, we can write the ratio of the two fluxes as

$$\frac{J_{(4)}}{J_{(3)}} = p_{3 \rightarrow 4} < 1. \quad (\text{S46})$$

Therefore, the 4-filter trajectory is necessarily slower than the 3-filter one and cannot dominate the dynamics of wrong product formation.

Now let us look at the slightly more complicated second example. There the fluxes of the 4-filter and 1-filter trajectories are

$$J_{(4)} = \pi_0 k_{0 \rightarrow 1} \times p_{1 \rightarrow 2} p_{2 \rightarrow 3} p_{3 \rightarrow 4} p_{4 \rightarrow 5} \times p_5^{\text{cat}}, \quad (\text{S47})$$

$$J_{(1)} = \pi_0 k_{0 \rightarrow 1} \times p_{1 \rightarrow 6} \times p_6^{\text{cat}}, \quad (\text{S48})$$

respectively. The full expression of the transition probability  $p_{4 \rightarrow 5}$  is

$$p_{4 \rightarrow 5} = \frac{k_{4 \rightarrow 5}}{k_{4 \rightarrow 5} + k_{4 \rightarrow 3} + k_{4 \rightarrow 1} + k_{4 \rightarrow 7}}. \quad (\text{S49})$$

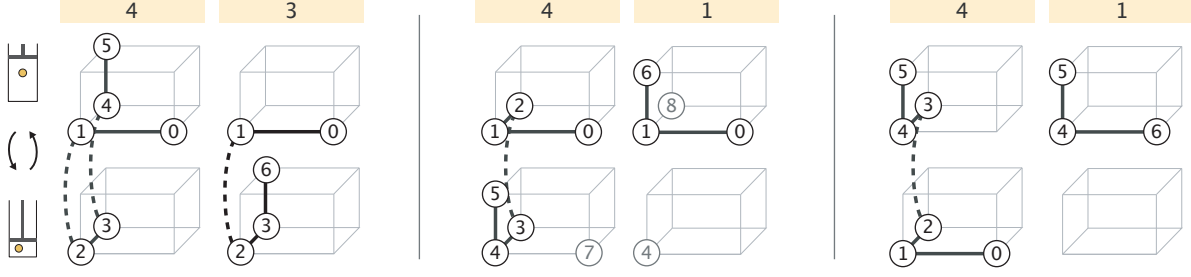


**Figure S12.** Three representative 4-filter trajectories paired with ones which have a lower filter number and, necessarily, a higher product formation flux. The state indices are added to facilitate the comparison between the corresponding trajectories.

Similarly, the expression for  $p_{1 \rightarrow 6}$  is

$$p_{1 \rightarrow 6} = \frac{k_{1 \rightarrow 6}}{k_{1 \rightarrow 6} + k_{1 \rightarrow 8} + k_{1 \rightarrow 4} + k_{1 \rightarrow 0}}. \quad (\text{S50})$$

All corresponding rates in the above probability expressions are equal to each other (i.e.  $k_{4 \rightarrow 5} = k_{1 \rightarrow 6} = k_{\text{A}}^{\text{S}}$ ,  $k_{4 \rightarrow 1} = k_{1 \rightarrow 4} = k_{\text{b}}$ ,  $k_{4 \rightarrow 7} = k_{1 \rightarrow 0} = k_{\text{off}}^{\text{W}}$ ), with the exception of  $k_{4 \rightarrow 3} = \ell_{\text{on}}^{\text{I}}[\text{L}]_{\text{d}}$  and  $k_{1 \rightarrow 8} = \ell_{\text{on}}^{\text{I}}[\text{L}]_{\text{u}}$ . Now, since  $[\text{L}]_{\text{d}} > [\text{L}]_{\text{u}}$ , we obtain  $p_{4 \rightarrow 5} < p_{1 \rightarrow 6}$ . With an identical reasoning we can also find that  $p_5^{\text{cat}} < p_6^{\text{cat}}$ . Therefore, the ratio of the 4-filter and 1-filter trajectory fluxes becomes

$$\frac{J_{(4)}}{J_{(1)}} = p_{1 \rightarrow 2} p_{2 \rightarrow 3} p_{3 \rightarrow 4} \underbrace{\left( \frac{p_{4 \rightarrow 5}}{p_{1 \rightarrow 6}} \right)}_{<1} \underbrace{\left( \frac{p_5^{\text{cat}}}{p_6^{\text{cat}}} \right)}_{<1} < 1, \quad (\text{S51})$$

proving our claim.

Lastly, we consider the third example in Figure S12. We again start off by writing the trajectory fluxes, namely,

$$J_{(4)} = \pi_0 k_{0 \rightarrow 1} \times p_{1 \rightarrow 2} p_{2 \rightarrow 3} p_{3 \rightarrow 4} p_{4 \rightarrow 5} \times p_5^{\text{cat}}, \quad (\text{S52})$$

$$J_{(1)} = \pi_6 k_{6 \rightarrow 4} \times p_{4 \rightarrow 5} \times p_5^{\text{cat}}. \quad (\text{S53})$$

The two rates appearing in the flux expression represent the substrate binding rate and are equal to each other, that is,  $k_{0 \rightarrow 1} = k_{6 \rightarrow 4} = k_{\text{on}}^{\text{I}}[\text{S}]$ . Now, note that  $\pi_6$  is the steady state probability of the inactive ligand-unbound enzyme state at a low ligand concentration, whereas  $\pi_0$  is the probability of the same enzyme state at a high ligand concentration. Since these are ligand-unbound states, the one in the presence of a lower ligand concentration will have a higher probability, i.e.  $\pi_6 > \pi_0$ . Thus, taking the ratio of the two fluxes, we obtain

$$\frac{J_{(4)}}{J_{(1)}} = \underbrace{\left( \frac{\pi_0}{\pi_6} \right)}_{<1} p_{1 \rightarrow 2} p_{2 \rightarrow 3} p_{3 \rightarrow 4} < 1, \quad (\text{S54})$$

suggesting that the 4-filter trajectory in the third example too cannot be the dominant one.

## References

- (1) Feynman, R. P.; Leighton, R. B.; Sands, M. *The Feynman Lectures on Physics*; Addison-Wesley: Reading, MA, 1963; Vol. 1.
- (2) Magnasco, M. O.; Stolovitzky, G. Feynman's Ratchet and Pawl. *J. Stat. Phys.* **1998**, *93*, 615–632.
- (3) Hill, T. L. *Free Energy Transduction in Biology: The Steady State Kinetic and Thermodynamic Formalism*; Academic Press, 1977.
- (4) Schnakenberg, J. Network Theory of Microscopic and Macroscopic Behavior of Master Equation Systems. *Rev. Mod. Phys.* **1976**, *48*, 571.
- (5) Horowitz, J. M.; Zhou, K.; England, J. L. Minimum Energetic Cost to Maintain a Target Nonequilibrium State. *Phys. Rev. E* **2017**, *95*, 042102.
- (6) Hopfield, J. J. Kinetic Proofreading: A New Mechanism for Reducing Errors in Biosynthetic Processes Requiring High Specificity. *Proc. Natl. Acad. Sci. U.S.A.* **1974**, *71*, 4135–4139.
- (7) Murugan, A.; Huse, D. A.; Leibler, S. Discriminatory Proofreading Regimes in Nonequilibrium Systems. *Phys. Rev. X* **2014**, *4*, 021016.